Robin S. Marjoribanks*, Christian Dille, Joshua E. Schoenly, Luke McKinney, Aghapi Mordovanakis, Patrick Kaifosh, Paul Forrester, Zuoming Qian, Andrés Covarrubias, Yuanfeng Feng and Lothar Lilge

Ablation and thermal effects in treatment of hard and soft materials and biotissues using ultrafast-laser pulse-train bursts

Ablation und thermische Effekte bei der Bearbeitung von harten und weichen Materialien sowie Biogewebe mittels ultraschneller Laserimpulsfolgen

Abstract: Ultrafast laser pulses (≤1 ps) are qualitatively different in the nature of their interaction with materials, including biotissues, as compared to nanosecond or longer pulses. This can confer pronounced advantages in outcomes for tissue therapy or laser surgery. At the same time, there are distinct limitations of their strong-field mode of interaction. As an alternative, it is shown here that ultrafast laser pulses delivered in a pulse-train burst mode of radiant exposure can access new degrees of control of the interaction process and of the heat left behind in tissues. Using a laser system that delivers 1 ps pulses in 20 µs pulse-train bursts at 133 MHz repetition rates, a range of heat and energy-transfer effects on hard and soft tissue have been studied. The ablation of tooth dentin and enamel under various conditions, to assess the ablation rate and characterize chemical changes that occur, are reported. This is compared to ablation in agar gels, useful for live-cell-culture phantoms of soft tissues, and presenting different mechanical strength. Study of aspects of the optical science of laser-tissue interaction promises to make qualitative improvements to medical treatments using lasers.

Keywords: laser-ablation; absorption; burst-mode.

Zusammenfassung: Ultraschnelle Pulse (≤1 ps) unterscheiden sich von Nanosekunden- oder noch längeren Pulsen qualitativ in der Art ihrer Wechselwirkung mit Materialien, einschließlich Biogewebe. Dies kann in der Gewebetherapie oder in der Laserchirurgie von Vorteil sein. Andererseits gibt es klare Einschränkungen hinsichtlich ihrer Starkfeld-Effekte. Als Alternative wird in der vorliegenden Arbeit gezeigt, dass ultraschnelle Pulse, die im sogenannten Burst-Modus der Bestrahlung abgeben werden (d.h. in einer schnellen Folge stoßweise ausgesendeter Impulse oder Pulszüge) dazu beitragen können, den Wechselwirkungsprozess und die dabei erzeugte Wärme besser zu kontrollieren. Dazu wurden die Wärme- und Energietransfereffekte an Hart- und Weichgewebe untersucht, die mittels eines Lasersystems erzeugt wurden, mit dem 1 ps-Pulse in 20 µs-Impulsfolgen mit einer Wiederholrate von 133 MHz abgegeben wurden. Es wird über Ablationsversuche an Dentin und Zahnschmelz unter verschiedenen Bedingungen berichtet, die mit dem Ziel durchgeführt wurden, die Ablationsrate zu evaluieren und auftretende chemische Veränderungen zu charakterisieren. Die Ergebnisse wurden mit der Ablation in Agargels verglichen, die gut als Weichgewebephantome geeignet sind und eine unterschiedliche mechanische Festigkeit aufweisen. Insgesamt verspricht die Untersuchung der optischen Aspekte der Laser-Gewebe-Wechselwirkung eine qualitative Verbesserung von medizinischen Laseranwendungen.

Schlüsselwörter: Laserablation; Absorption; Burst-Modus.

*Corresponding author: Robin S. Marjoribanks, Department of Physics and Institute for Optical Sciences, University of Toronto, 60 St. George Street, Toronto ON, M5S 1A7, Canada, E-mail: marj@physics.utoronto.ca

Christian Dille: Department of Physics and Institute for Optical Sciences, University of Toronto, 60 St. George Street, Toronto ON, M5S 1A7, Canada

Joshua E. Schoenly: Department of Physics and Institute for Optical Sciences, University of Toronto, 60 St. George Street, Toronto ON, M5S 1A7, Canada

Luke McKinney: Department of Physics and Institute for Optical Sciences, University of Toronto, 60 St. George Street, Toronto ON, M5S 1A7, Canada

Aghapi Mordovanakis: Department of Physics and Institute for Optical Sciences, University of Toronto, 60 St. George Street, Toronto ON, M5S 1A7, Canada

Q1:
Please confirm running head.

Patrick Kaifosh: Department of Physics and Institute for Optical Sciences, University of Toronto, 60 St. George Street, Toronto ON, M5S 1A7, Canada

Paul Forrester: Department of Physics and Institute for Optical Sciences, University of Toronto, 60 St. George Street, Toronto ON, M5S 1A7, Canada

Zuoming Qian: Department of Physics and Institute for Optical Sciences, University of Toronto, 60 St. George Street, Toronto ON, M5S 1A7, Canada

Andrés Covarrubias: Department of Physics and Institute for Optical Sciences, University of Toronto, 60 St. George Street, Toronto ON, M5S 1A7, Canada

Yuanfeng Feng: Department of Physics and Institute for Optical Sciences, University of Toronto, 60 St. George Street, Toronto ON, M5S 1A7, Canada

Lothar Lilge: Ontario Cancer Institute and Department of Medical Biophysics, University of Toronto, 610 University Ave., Toronto ON, M5G 2M9, Canada

1 Introduction

In laser ablation of soft or hard biological tissues using lasers, energy absorption and heat transfer are determining factors for regulating the ablation process and for controlling collateral effects that may damage or stimulate living tissues. When ablating hard tissue, such as dental enamel, some heat transfer to the surrounding hard tissue may be desirable since melting may produce helpful material modifications [1]. However, when ablating soft tissue it is often important to minimize heat transfer to avoid damage to healthy tissue, or delay of wound healing. For instance, in refraction-corrective surgery, nanosecond (ns) laser pulses of a particular wavelength and radiant exposure may produce gross absorption and heating within a tissue, launching shockwaves which kill non-replicating epithelial cells on the inside of the cornea, eventually thinning their layer [2]. Ultrafast laser pulses (≤ 1 ps) are recognized to reduce thermal and shock effects [3–6], but may still have collateral effects of their own, originating with the more-intense optical fields produced in a shorter-duration pulse of comparable energy.

Long-pulse (≥ 10 ps) and continuous wave (cw) lasers interact with hard and soft tissues through linear absorption, leading to prompt heating within an absorption depth, and delayed heating over a range determined by thermal conductivity, and subsequently leading to ablation. Lasers having high average power nominally offer high ablation rates. However, in hard tissues [7, 8] relatively low thermal conductivity can cause thermo-mechanical stress fractures [9], which ultimately lead to less-precise ablation and to potential sites for infection [10, 11]. In soft tissues extensive charring and carbonization of the tissue can result, which may delay healing.

Absorption of ultrafast laser pulses is a little more complex process, yet ultimately simpler: for most typical applications the principal distinction is that, for a given radiant exposure, as the pulse duration is shortened the intensity is increased concomitantly. In dielectric materials and typically in tissues, field strengths are reached which ionize the medium by a combination of multiphoton absorption and avalanche ionization [3, 4]. Thereafter, absorption is mediated by the moderately dense plasma that is formed, which has its own characteristic absorption, relatively independent of the wavelength. Thus, though the process starts as a non-linear one, once plasma-mediated absorption has been established subsequent absorption is a linear process, but one in which the specific chromophores of the tissue or other medium matter little.

To the degree that ultrafast-laser ablation is determined by plasma-mediated absorption, generically, and subsequently by the thermal properties of the medium, what can be learned from ultrafast-laser materials-processing largely carries over to hard and soft biotissues. In materials-processing studies, solutions using ultrafast-laser pulses at high repetition rates (>1 MHz) have been found which permit high rates of ablation while greatly reducing material stress – and with little post-exposure strain left behind in the material [12]. Those studies suggest important new directions for clinical laser treatments of dental enamel and dentin, and perhaps of bone.
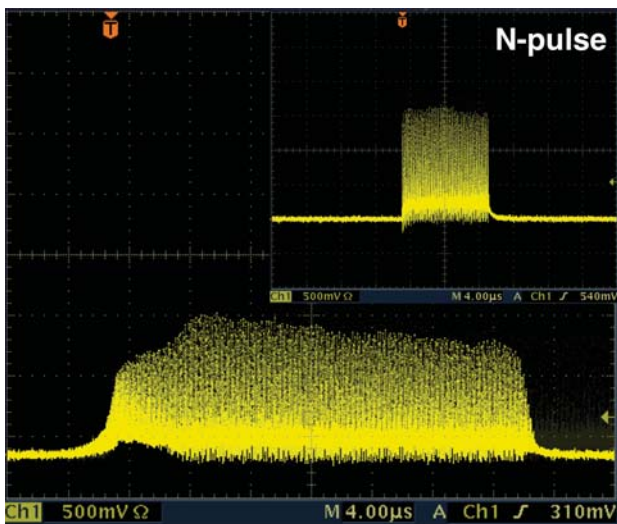
This paper compares the impact of ultrashort (≤ 1 ps) laser pulses at high repetition rates (multi-MHz) on soft, hard, and brittle materials and on soft and hard biotissues. It is seen that this 'ultrafast-laser pulse-train burst' mode of delivery of radiant exposure permits ablation at levels below the normally expected threshold for isolated pulses, permitting somewhat gentler material removal. While interaction has the low collateral impact characteristic of ultrafast lasers, small amounts of residual heat build up slowly and modify material characteristics during processing. In the case of brittle materials and tissues, this means that shocks and ablation take place not in the original brittle state, but in context of a temporarily more ductile medium, reverting to a brittle medium after processing. This gives the ultrafast-laser pulse-train burst mode a special niche in hard-tissue treatments, e.g., for dental surgery. In the case of soft tissues, this offers new avenues of control for laser ablation or debridement, especially for restricting undesirable collateral heating, or optimizing circumstances of desirable collateral heating.
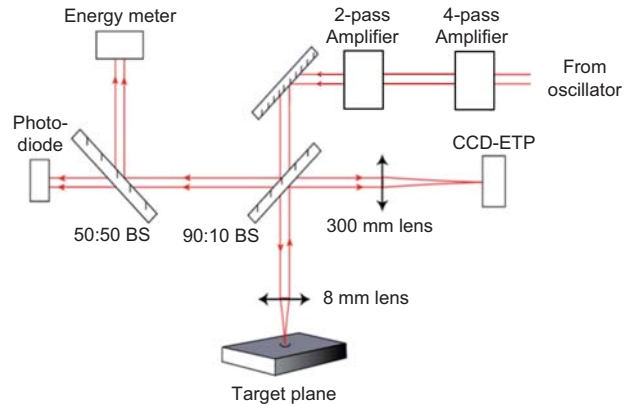
2 Materials and methods

2.1 Laser system

The laser used in the studies reported here is a purpose-built flashlamp-pumped Nd: glass system (λ=1054 nm) at the University of Toronto [13]. An oscillator with active-passive and feedback-controlled mode-locking produces a quasi-cw pulse-train burst of over 3000 pulses, with pulse durations adjustable in the range of 1–10 ps (Figure 1). Direct from the oscillator, intrinsic pulse energies are up to 1 µJ (typically 100 nJ) with inter-pulse separations of 7.5 ns (133 MHz). The pulse-train burst duration is up to 20 µs per shot.

Shorter pulse-train bursts can be obtained using a purpose-built Pockels cell '*N*-pulse selector', which provides a square-pulse optical transmission window to select a sub-train (Figure 1, inset). Two multi-pass Nd: glass amplifiers increase the per-pulse energy to up to 10 µJ/pulse, and thus a total train energy of up to, e.g., 12 mJ per shot for a 10-µs burst (Figure 2). For studies of ultrafast pulse-train-burst treatment of metals, the beam was focused by under-filling a molded aspherical lens (Geltech C280TME; Thorlabs USA) with a numerical aperture (NA) of 0.15 and a focal length f≈18.4 mm, producing a focal spot of 7 µm full width at half maximum (FWHM). For studies of treatment of dielectrics (fused silica, dentin and enamel, and hydrogels), the beam was focused by under-filling a molded aspherical lens (Geltech C240TME;

Figure 2 Experimental setup for ablation with ultrashort pulse-train bursts. Back-reflected light is sampled to image the laser focal spot (equivalent-target plane, ETP).

Thorlabs USA) with NA=0.5 and a focal length f≈8 mm, making a focal spot measured to be 2 µm×3 µm FWHM. Optimal focusing was constantly monitored by autocollimating the retro-reflected beam, from which an equivalent-target plane (ETP) image was recorded on each shot. Pulse and total energies, pulse-train burst duration, and the pulse-train burst envelope were recorded for each shot using time-resolving and time-integrating photodiodes coupled with integrating spheres and similar. All irradiation of specimens was performed in air, with the laser at normal incidence onto the specimen surface.

For hydrogel tissue-proxy studies, the pulse-train burst was amplified using two four-pass amplifiers to reach a maximum per-pulse energy of ~30 µJ, and total per-shot (i.e., whole pulse-train burst) energies up to 80 mJ. The amplified pulse-train burst was focused onto the gel sample surface using a 20 mm focal length aspherical lens (Asphericon AL2520B; Thorlabs USA) to a near-diffraction-limited ~5-µm FWHM spot. Maximum available intensity at focus was 1.5×10^{14} W cm^{-2}. As before, ETP imaging provided a monitor of the size and quality of the focal spot. Unlike other specimens, each gel sample was irradiated with just one pulse-train burst (shot), to simplify interpretation.

2.2 Targets and target preparation

Metal-foil targets were compared to targets of fused silica, human tooth dentin and enamel, and hydrogels suitable for suspended cell-cultures.

Aluminum targets of thickness 10–200 µm (purity 99% or better; Goodfellow Corp., USA) were mounted on 2-mm thick holder-plates, the foils free-standing over 8 mm-diameter clearance holes.

Figure 1 Digital oscilloscope trace of the pulse-train burst ultrafast-laser output: 10–3000 pulses, 1–10 ps each, 7.5 ns between pulses (133 MHz); up to 10 µJ/pulse (after amplification from amplifier scheme in Figure 2) and 15 mJ/pulse-train burst. An N-pulse Pockels cell slicer controls duration of the burst (inset). (Irregularities are due to sampling aliasing.)

Fused silica (Corning 7980 UV Grade) targets were optically polished to a specification of 20/10 scratch/dig <7 Angstroms.

Sterilized extracted human teeth were obtained from the Department of Dentistry at the University of Toronto. Without decalcification, the clinical crowns were sectioned perpendicular to the long axis into 1 mm-thick slices using a diamond saw and then polished to about wavelength flatness. To ensure that the cutting and polishing process did not alter the chemical composition or structure, micro-Raman analysis (JY LabRAM; Horiba Scientific, USA) on the prepared enamel and dentin was performed.

All targets were positioned at focus to within a Rayleigh range, as monitored by the ETP system described above and in Figure 2.

Hydrogels were prepared by dissolving solid agar in distilled water at a concentration of 25 µg/ml and temperature of 45°C, leaving them to solidify at room temperature. Punch-hole biopsies, 6 mm in diameter, were extracted from the hydrogel for laser irradiation. In order to facilitate virtual sectioning by confocal fluorescence laser scanning microscopy (CFLSM), as discussed below, hydrogels were prepared with the addition of rhodamine-123.

2.3 Diagnostics and analysis

After laser irradiation, optical micrographs of all specimens were made for preliminary examination, before glass, dentin and enamel specimens were coated by evaporation-deposition with a 300 nm-thick layer of gold for scanning electron microscopy (SEM) (Hitachi S-2500). Stereoscopic SEM images were taken by tilting the samples eucentrically by 2–5° around the ablated site at the surface plane, and a three-dimensional (3D) digital elevation model (DEM) was created using a post-processing stereoscopic

analysis package (MeX®; Alicona Imaging GmbH, Austria) [14]. The virtual object gave the 3D morphology (Figure 3) with a systematic accuracy of about 3% (typ.±1 µm) in depth, from which ablated width, height and volume could be measured.

After laser irradiation, hydrogels prepared with rhodamine-123 were mapped in 3D using a confocal laser scanning microscope (LSM 510; Zeiss, Germany) with an objective (FLUAR; Zeiss) having a 10×magnification, 0.5 NA, and 1.9-mm-long working distance sufficient to access fluorophores deep within the hydrogel matrix.

3 Results

For ultrafast laser pulses and absorption by plasma-mediated ablation, plasma absorption is 'generic' and whether for hard or soft biotissues, glass, or metals the plasma is metal-like in its optical characteristics. The principle distinctions in how the specimen is subsequently affected lie in the material properties: thermal diffusivity, specific heats of melting and vaporization, and mechanical properties such as tensile strength and shear strength. Results in fused silica are particularly useful, since the material is dielectric, but questions remain, in comparison to hard and soft tissues, about the contributions of linear absorption, and the propagation of heat and shock waves.

3.1 Comparison of single-pulse and burst mode in dielectric material

Figure 4 compares the depth of etching in fused silica which resulted from irradiation by 1-ps pulses, delivered
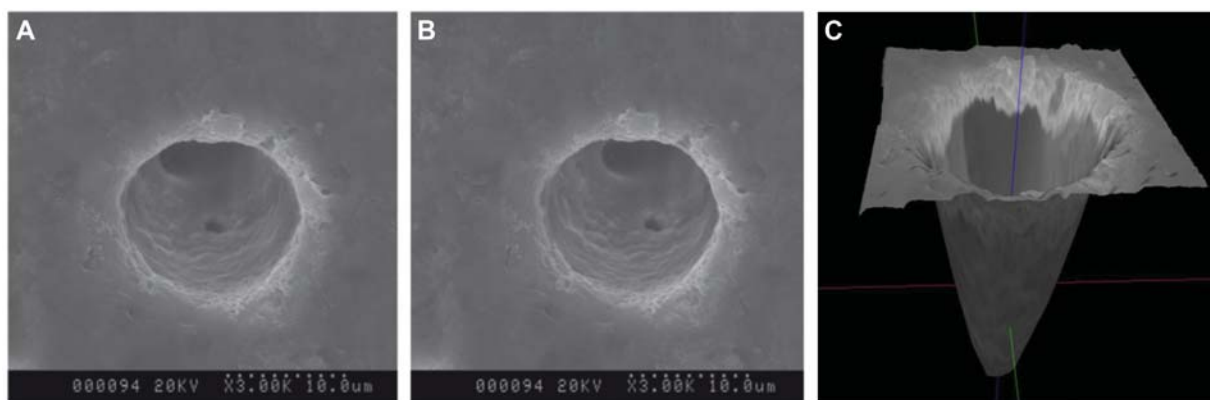
Figure 3 (A) and (B): Stereoscopic SEM images of human tooth irradiated by 10 µs pulse-train burst. (C): 3D digital elevation model created in MeX® from the stereoscopic pair.
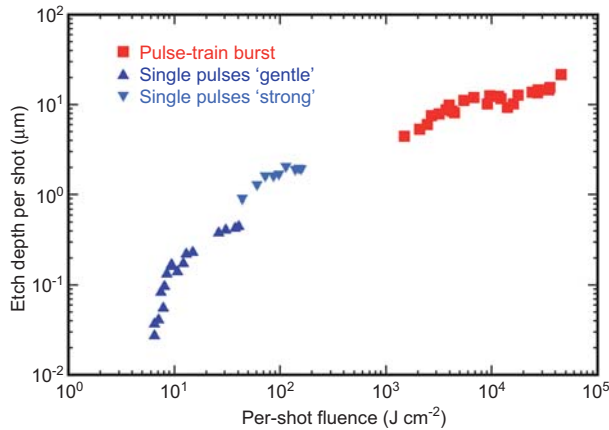
Figure 4 Fused silica etch rates – single 1-ps pulses vs. pulse-train burst mode, as a function of total fluence delivered. For single pulses, a gentle-etch regime spans fluences of 7–60 J cm^{-2}; a strong-etch regime spans fluences of 60–200 J cm^{-2}. Above 200 J cm^{-2}, single shots fracture the fused silica, burst-mode does not.

singly or in bursts of 300 pulses at 7.5-ns spacing between pulses. Here, the etch depth of ablation (measured in profile from optical microscopy) is plotted against the total fluence (radiant exposure) which produced it. With single 1-ps pulses, two characteristic regimes of etching or ablation of glass are evident: a so-called gentle-etch regime (up to about 60 J cm^{-2}), and a strong-etch regime (in the range 60–200 J cm^{-2}).

For 1-ps single-pulse ablation, 200 J cm^{-2} was a limit corresponding to etch-depths of a few micrometers. Above this single-pulse fluence, the fused silica specimen typically would shatter in a single shot (illustrated in Figure 5A). Even below this fluence, it was possible to accumulate only a limited number of weaker etching shots (<1 Hz) before shattering the glass, more shots for weaker pulses before fracture. The net effect was that single pulses acting at the same location ultimately could not etch more

deeply than a few micrometers, whether delivered in a single strong pulse or via multiple weaker shots [15].

This was contrasted with the effect of a train of 300 1-ps pulses delivered at 133 MHz, which etched to several tens of micrometers in one 300-pulse shot. These etch depths are deeper than those achieved by overlapping single shots and at per-shot fluences of 1–60 kJ cm^{-2}, well beyond the limit at which a single pulse shattered the fused silica. Figure 5B illustrates the qualitatively different morphology which results: an optically smooth bore, and lip of material apparently raised while the material was ductile.

Cast in another way, Figure 6 compares what each individual pulse ablates, whether singly or on average in context of a burst of pulses (for pulse-train burst data points in Figure 6 the total fluence and the total etch-depth have been divided by the number of pulses). Here the relationship is reversed: within a pulse-train, each pulse can accomplish relatively gentle ablation at a per-pulse fluence an order of magnitude less than the nominal threshold for single pulses as seen in Figure 4.

3.2 Ablation rates in dentin and enamel

In context of the differences between single-pulse and pulse-train burst treatment of fused silica, the etch-depth and volume ablation rates in dentin and enamel using pulse-train burst mode are particularly interesting.

Human dentin specimens were irradiated at low (2 J cm^{-2}) and high (4 J cm^{-2}) radiant exposures per individual pulse, with varying pulse-train lengths of 3, 6, 8, 12, and 15 μs. Depths of etched hole were measured from DEMs produced stereoscopically, as described earlier. Figure 7 depicts the relationship of hole depth to pulse-train burst duration: hole depth increases, as expected, with both
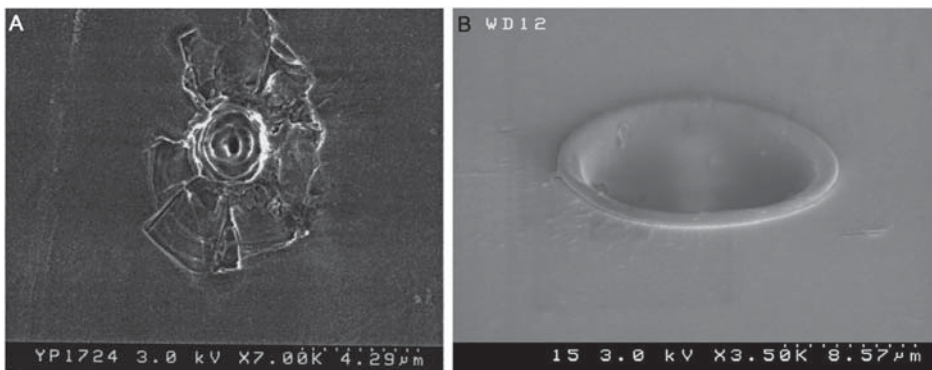

Figure 5 SEM top-view micrograph of microcracks in fused silica in usual ultrafast interaction: four individual 1-ps λ=1 μm pulses at 93 J cm^{-2} fluence at a frequency of 1 Hz (A). View of hole in BK7 glass made by one burst-machining shot, using 300 1-ps λ=1 μm pulses. The ~15-μm deep hole has smooth walls and shows no evidence of fractures, cracks, or collateral damage (B).
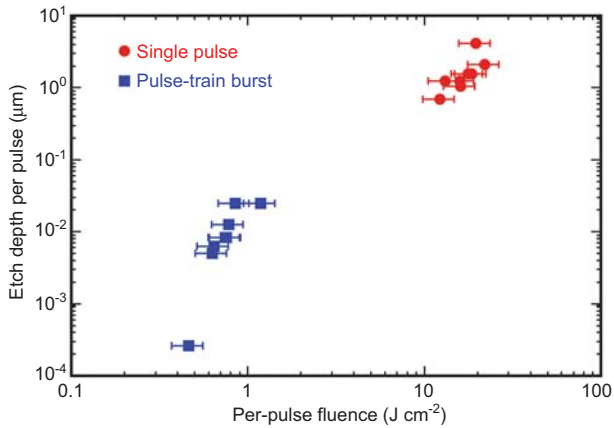
Figure 6 Etch-rate per individual pulse: etch depth per pulse, of a train of N pulses, is taken as the average: (net depth)/N; fluence per pulse is taken as the average (integrated fluence)/N. On a per-pulse basis, pulse-train burst is extremely gentle.

pulse-train burst duration and integrated (whole-burst) radiant exposure.

The volume rate of removal of material is an important metric for practical surgical and dental applications. As previously reported elsewhere [7], a conventional 1 kHz Ti: sapphire fs-laser system with per-pulse energies of ≈1 mJ provides steady volumetric ablation rates of ≈2 mm^3 s^{-1} under identical focusing conditions as used in the present studies (i.e., per-pulse radiant exposure of 16 kJ cm^{-2}). In the present study, ultrafast-laser pulse-train burst processing of dentin using a 15-μs-duration pulse-train burst with average per-pulse energy of 2 μJ, average (i.e., total energy 4 mJ; total fluence 67 kJ cm^{-2}; per-pulse radiant exposure 33 J cm^{-2}; peak intensity 2.4×10^{13} W cm^{-2}), resulted in an average volumetric ablation rate of 3×10^3
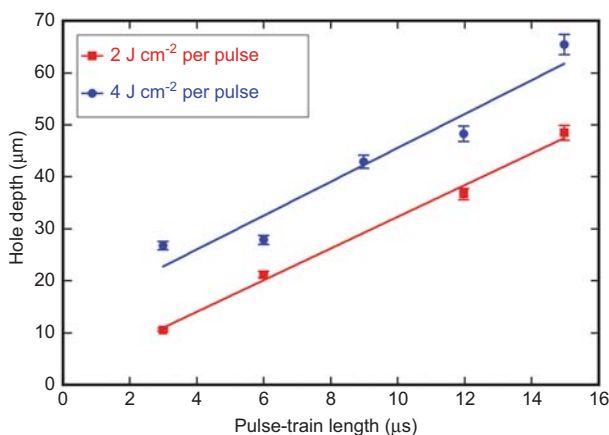
Figure 7 Measured hole depths in dentin, vs. pulse-train burst duration (1 μs=133 pulses), for per-pulse fluences of 33 J cm^{-2} (peak intensity 2.4×10^{13} W cm^{-2}). A one-shot ablation depth of 65 μm resulted for 15 μs pulse-train bursts.

mm^3 s^{-1} during irradiation. Compared to the 1-kHz Ti: sapphire laser in [7], pulse-train burst processing is 3×10^{-3} the per-pulse radiant exposure, delivered at 1.3×10^5 the repetition rate. For comparison, a conventional high-speed dental drill will remove material at a much slower rate of about 1 mm^3 s^{-1} [16].

3.3 Test of modes of delivery of radiant exposure – fluence division

The observed differences between modes of delivery – single or kHz pulse rates and multi-MHz rates – begs the question about how one pulse affects the absorption of another, when mediated by timescales of the material or of the plasma. In laser materials processing of crystalline and amorphous solids important in photonics and industrial applications, a well-known effect is that of latent damage or subtle modification by the 'incubation' of crystal defects or structural changes [17]. For instance, in metals there is evidence that by irradiation with many pulses, just below the catastrophic damage threshold, crystal dislocations can be accumulated in the bulk. These occur over the depth of heat diffusion, accumulating over many shots before gross damage is manifest. In some dielectrics, color centers can be developed at irradiation intensities insufficient for ablation. Such preconditioning of the material is thought to affect subsequent ablation damage thresholds, and may well be a factor that affects pulse-train burst mode treatments.

On the premise that for pulse-train burst interactions the target effectively mediates interaction between pulses, incubation effects were investigated by introducing the principle of 'fluence division' – delivering a constant integrated fluence, but dividing it into separate bursts to restart the interaction each time.

For this investigation, total fluence was kept constant for all series. Then this constant total fluence was delivered in different ways: as one burst of 12 μs, two bursts of 6 μs, three bursts of 4 μs, and four bursts of 3 μs, with a delay of seconds between bursts to ensure complete relaxation of the processes involved. Thus, a pulse-train burst of 1600 pulses was divided into N smaller mini-bursts, each with n pulses, where $N\cdot n$=1600. The efficiency of etching, for each of these ways of delivering 1600 pulses, was compared.

The results are shown for fused silica in Figure 8, and for human dentin in Figure 9. As the fixed total fluence was delivered in more numerous and progressively shorter pulse-train bursts, shallower etch-depths resulted. Clearly, the more interrupted the fluence
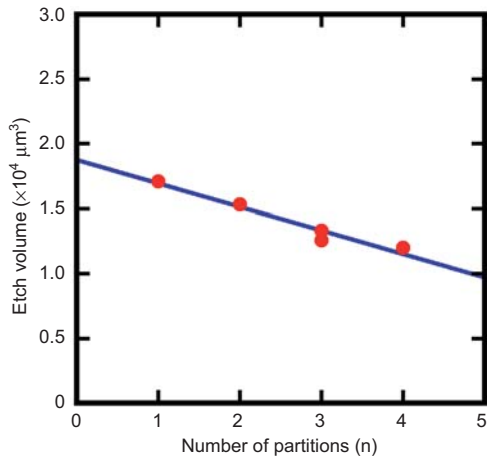
Figure 8 Fluence-division effect in fused silica: overall fluence delivered to each site was kept constant while partitioning a pulse-train burst of 1600 pulses into separate shots: 2×800, 3×533, and 4×400. 'Restarting' the ablation process imposes a cost on ablated volume each time, equivalent here to ~155 pulses lost from the beginning of the pulse-train burst. Total fluence was fixed at 18 kJ cm^{-2}.

delivery, i.e., the more times re-starting the laser-matter interaction, the greater the fraction of fluence that went into preconditioning the tissue without ablating it. The trend may be explained by considering the number of pulses which remain to do the etching, in each case, after a fixed number of conditioning or incubating pulses have been 'deducted' from ablation.

This can be modelled as follows: suppose that a fixed number a of pulses must be 'invested' at the start of each
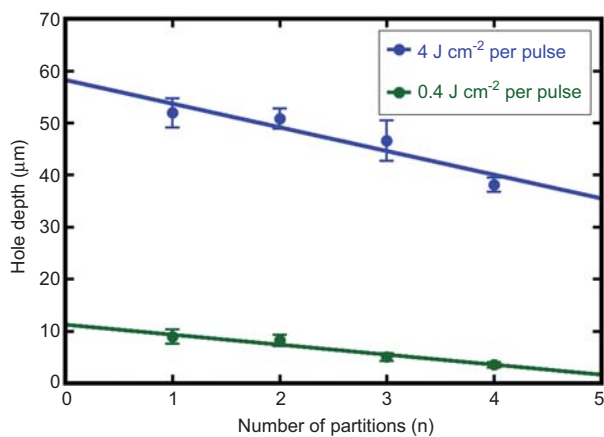
Figure 9 Fluence-division effect in dentin: overall fluence delivered to each site kept constant while partitioning 1600 pulses into separate shots: 2×800, 3×533, 4×400, etc. 'Restarting' the etching process imposes a cost, each time, equivalent to ~280 pulses lost for the lower-intensity interaction and ~130 pulses lost for the higher-intensity interaction. Total fluences were fixed at 54 kJ cm^{-2} (blue curve) and 5.4 kJ cm^{-2} (green curve).

pulse-train burst, before ablation substantially begins. If one has a total number A of pulses, and partition those into N mini-bursts, $N·a$ pulses are lost as 'overhead' to seed the ablation process, leaving $A−N·a$ pulses to do the etching. If these etch with equal efficiency, once the material has been preconditioned, then the net etch-depth will scale as A-N·a.

For fused silica in Figure 8, this scaling fits the data very well, implying that 155 pulses are invested at the start of each processing-burst: the more times the pulse-train is restarted, the greater the 'cost'. From dentin in the lower-fluence data of Figure 9, the fit implies that processing is latent for approximately the first 300 pulses of each mini-burst. For the higher-intensity case, a similar fit suggests a latency of about 128 pulses. Together, these results suggest that under these conditions ablation does not begin immediately, and some effect similar to incubation is in play, in which the material heats, the density of plasma builds, or the material itself changes composition. This process must be reversible, though, in the sense that re-starting the pulsetrain restarts the process.

3.4 Range of residual heat

As discussed above, for nanosecond and longer-duration laser pulses, the heat-affected zone around the focal spot can be large, and significant collateral damage can be imposed in materials, corresponding to significant histological insult in tissues. It is recognized that ultrafast-laser pulses, by virtue of their brief duration, produce far less collateral impact on the specimen. Given that pulse-train burst ultrafast laser treatments combine both timescales, making it unclear which category would be most similar, inference of heat-range was made in aluminum, a conductor with much larger thermal diffusion constant than dielectrics like fused silica, and dentin.

For this purpose, 100 μm-thick aluminum foils were pierced through by pulse-train bursts of 1600 pulses (12 μs) at fluences up to 6 kJ cm^{-2}, and ablated hole-sizes were recorded (Figure 10). With increasing fluence, the size of the hole drilled through increases, but not surprisingly this size does not match the radius under the Gaussian focal spot at which the specific energy imprinted matches the specific latent heat of vaporization – that is to say, ablation was not limited by local heat deposition. Instead, the much larger hole sizes can be fit by a dependence $E_0^{1/2}$ as shown in Figure 10. The physical reason for this scaling is discussed further in chapter "Discussion", section 4.3.
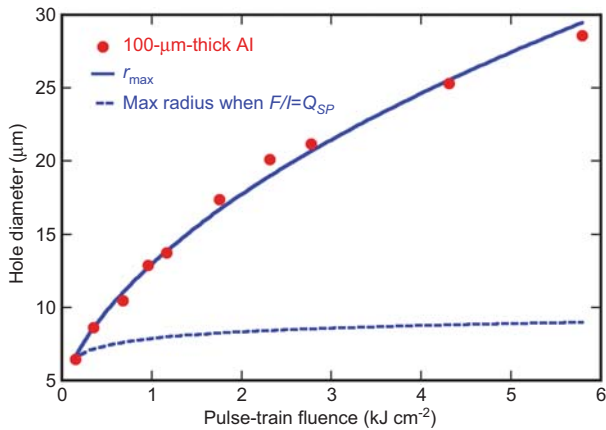
Figure 10 Experimental dependence of through-hole diameter against average irradiant exposure (fluence), for l=100 μm aluminum foils under pulse-train burst processing. Hole size is compared to two models: (A) the radius at which the Gaussian-beam locally 'prints' sufficient fluence F so that F/l equals the latent heat of vaporization; and (B) the maximum extent of a relaxing thermal distribution initially matching the laser profile, as measured at the threshold specific heat (compare with Figure 17).

3.5 Material modification

The mix of timescales, microsecond and picosecond, involved in pulse-train burst processing provides a special opportunity for controlling the way in which the total radiant exposure is delivered to the tissue. Whereas the pulse duration is short compared to characteristic thermal diffusion timescales, the pulse-train duration is relatively long compared to these and to hydrodynamic timescales for ablation. Therefore, one aspect of the study is the impact of pulse-train duration on collateral heating or specimen modification. Figure 5B shows detail of the lip of fused silica apparently melted and re-solidified, rather than recast, around the periphery of the treatment site;

Figure 11 shows SEM images of ablation sites in dentin for pulse-train durations of 5, 10, and 20 μs. It can be seen that the melting is more extensive with increasing pulse-train burst duration: the time over which heat is deposited is large, but the ablation – and the small heat taken up from each 1-ps pulse – has ultrafast-laser character.

3.6 Micro-Raman analysis

Through diffusion of heat, and potentially directly from ionization, extended material modifications can be caused during laser irradiation. This has previously been shown for dental hard tissue [1, 10], and has been recognized in changes of index of refraction in fused silica. Of particular relevance, others have shown [10] a potential for lasers to modify and strengthen enamel against corrosive agents (i.e., acid attack from dental caries) by heating the enamel above 400°C and removing carbonate constituents. Since dental caries concerns both enamel and dentin, micro-Raman spectroscopy (MRS) was used to assess material modification therein, and to compare changes in apatite mineral structures to those of the amorphous silicon dioxide.

Figure 12 shows the MRS spectrum of untreated fused silica, and compares it to the spectrum sampled for the remelted lip around the ablation crater (glass transition temperature about 1600 K). Changes in the bond-coordination statistics are evident, which may correspond to densification of the glass.

Figure 13 shows MRS spectra of untreated dentin (blue curve) and enamel (red curve), and compares them to the spectrum obtained for dentin that has been melted and redistributed, or ablated and re-deposited, around the ablation site (green curve). The clear peaks around 500 cm^{-1} and at 965 cm^{-1} correspond to the hydroxyapatite and
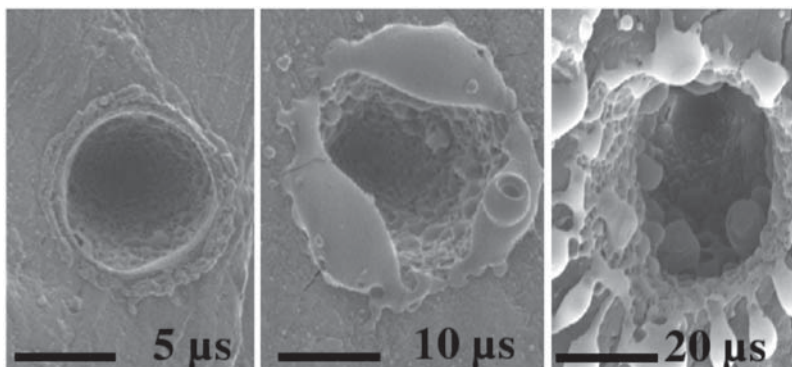
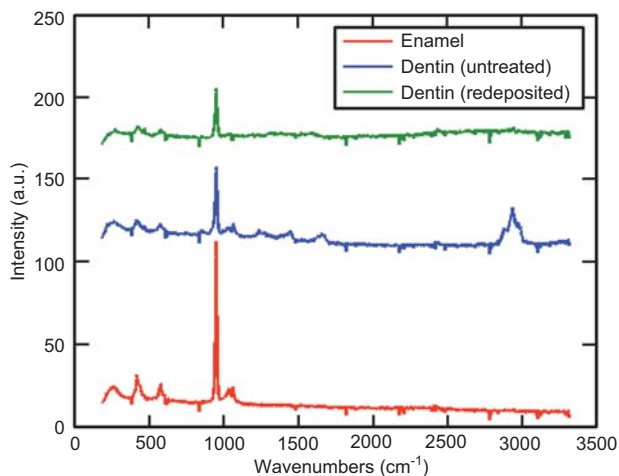**Figure 11** SEM images of dentin tissue irradiated with pulsetrains of the durations 5, 10, and 20 μs (22 kJ cm^{-2}, 44 kJ cm^{-2}, 67 kJ cm^{-2}, respectively). Heating and material modification takes place over times up to 20 μs, but still using ultrafast plasma-mediated absorption. Scale bars in each image are 5 μm.
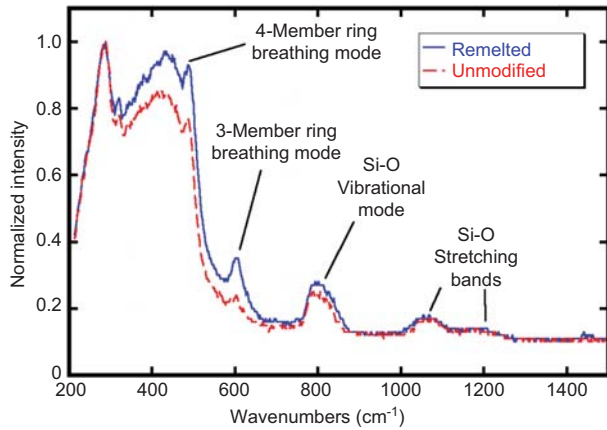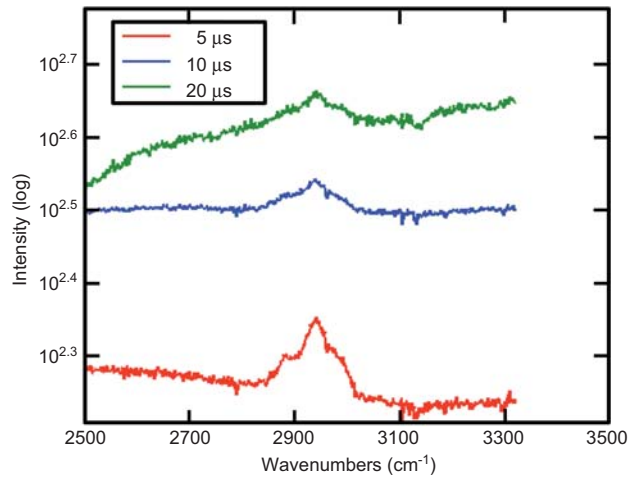
Figure 12 MRS of fused silica: the spectrum from unmodified glass far from the treatment site is compared to that from the smooth lip of glass around the ablated hole. MRS shows significant changes in the ring bond structures where the glass has been remelted.

Figure 14 MRS of the C-H component of dentin at 3000 cm^{-1}, treated by different length of pulse-trains (compare with Figure 11). As the pulse-train duration increases, the C-H peak is suppressed.

phosphate mineral components. Organic components of natural dentin are evidenced by the peaks at 1250–1661 cm^{-1} and 3000 cm^{-1}, which represent the collagen protein matrix of dentin and the carbon-hydrogen (C-H) bond, respectively. It is evident from Figure 13, that the modified dentin material has lost almost all its organic components following the melting and ablation process. Moreover, as the pulse-train burst duration is increased from 5 to 20 µs the C-H peak is progressively suppressed, as can be seen in Figure 14. It is likely that this follows vaporization of parts of the organic components due to the extreme heat generated during the melting or ablation process. This suggests that dentin in the flowed or re-deposited material has been purified and vitrified into an enamel-like material following laser irradiation.
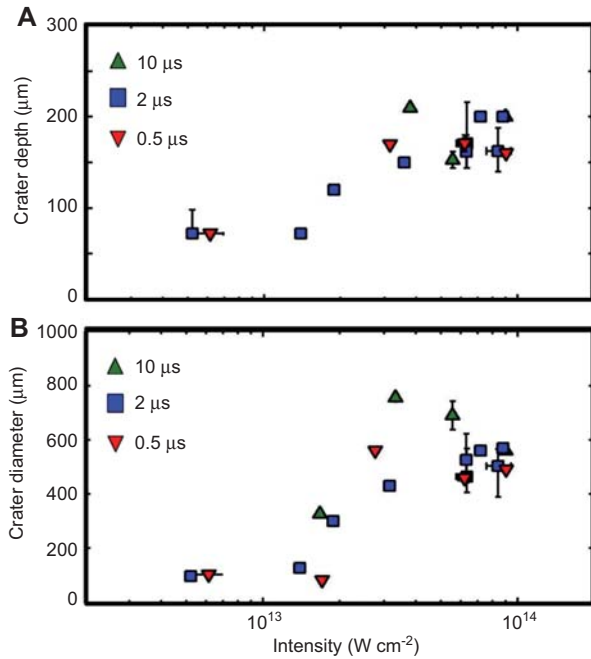
3.7 Soft tissue hydrogel model

Applied to soft tissues, the issues surrounding ultrafast laser ablation in general, and pulse-train burst ultrafast treatment in particular, are less about modification of the material left behind and more about the collateral impact on surviving cells around the crater. The fundamental mechanisms governing collateral cellular impact are best studied in a standardized tissue model that yields unambiguous, consistent results. Hydrogel cell cultures are commonly used as tissue proxies for laser-irradiation [18, 19] and fundamental studies of cell response to drug and radiation treatments (e.g., photodynamic therapy [20] and interstitial laser photocoagulation [21]).

The mechanical impact on hydrogels following pulse-train burst-mode laser ablation was investigated by measuring the volume of ablation craters, using CFLSM. Hydrogels have low optical scattering and absorption, and lend themselves well to virtual sectioning.

Ablation characteristics were found to be very reproducible. The crater depth, width and total volume were measured for different pulse intensities and burst durations (Figure 15). Both the the depth (Figure 15A) and the diameter measured at the surface (Figure 15B) of the ablation-crater scale nearly linearly with the per-pulse laser intensity over the range of 0.05–1.0×10^{14} W cm^{-2}.

There is, however, no discernible dependence on the pulse-train burst duration, in the range of 0.5–20 µs studied. Since it was expected that additional pulses should produce deeper craters, the time-dependent self-emission from the laser-induced plasma was measured. Green and blue self-emission light was recorded

Figure 13 MRS of enamel and of both untreated and pulse-train burst treated dentin. The modified dentin is glassy in appearance – MRS shows it has almost completely lost its organic components, the dentin vitrified as if enamel.

Figure 15 (A) depth and (B) diameter of the ablation crater in hydrogel as a function of per-pulse laser intensity (logarithmic scale) at several pulse-train burst durations shown in the figure legend.

for irradiating laser pulse-train durations of 0.1–20 μs, using the target lens to collimate light from the focus and relay it to a 1-ns risetime photodiode (DET210; Thorlabs USA). BG39 short-pass filters (Schott Glass, Germany) eliminated reflected 1053-nm laser light. Consistently, the plasma self-emission was observed to last for ~100 ns, regardless of the pulse-train burst duration. This indicates that in the case of hydrogels, unlike teeth, only the leading 10 to 13 pulses contribute to ablation. This suggests these initial pulses are sufficient to initiate plasma breakdown and then explosive boiling – to vaporize enough water to establish a low-density cavitation bubble in the gel, wider than the focal spot of the Gaussian beam (~5 μm) and as long as the Rayleigh range (~50 μm). The low tensile strength of these gels allows easy disruption, compared to dentin, glass and metals.

4 Discussion

Results show that the mode of delivery of radiant exposure, or fluence, does much to determine the impact of a given laser energy on a material or biotissue. Low repetition-rate (or single) ultrashort laser pulses leave only trace amounts of heat behind, but clearly with increasing repetition rate these trace amounts of heat have the potential to accumulate significantly [15], and

to thermally modify the specimen. This will depend on the degree to which the heat, and the plume of ablating plasma itself, dissipates during the delay between pulses.

4.1 Heat deposition and ablation

It appears that two factors allow these pulse-train bursts (at repetition rates greater 100 MHz) to etch more gently than single-pulse (1 Hz–100 kHz) etching – in fact, etching may proceed at a per-pulse fluence which is below the nominal threshold for single pulses to ablate glass.

One, the accumulation of heat in fused silica as in dentin and enamel, appears to temporarily modify the brittleness of the material, making it more ductile and less susceptible to shock fracture. The rapid repetition rate does not allow the material to cool between pulses, and inbuilt stresses from thermal cycling do not accumulate. Quantitatively, much deeper holes were made possible, from much greater per-shot (i.e., whole pulse-train burst) fluences of many tens of kJ cm^{-2}. On the microsecond timescale and micrometer spatial scale of the pulse-train burst irradiation here, this accumulated heat does not substantially dissipate; it is not simply that the laser energy is being delivered more slowly. Subsequently, the medium relaxes thermally and largely recovers its original state, with some exceptions here: bond-coordination rearrangement in fused silica, and ablation of the organic component of dentin, reorganizing the mineral component to be more like enamel.

Secondly, it appears likely that the repetition rate here is sufficiently high that plasma-mediated ablation may be persisting from pulse to pulse – that the ionized state does not fully relax to neutral, and therefore plasma-mediated ablation is kept 'simmering' between pulses. This may be part of the reason for the incubation-like behavior seen from fluence-division measurements, an incubation which nonetheless does dissipate on the longer timescale between pulse-train burst shots.

4.2 Ablative quenching

It is clear that in terms of heat-impact, treatment of tissues or materials with microsecond pulse-train bursts of ultrafast laser pulses does not look like treatment with microsecond laser pulses.

As discussed above, laser pulses of duration less than about 1 ps produce material removal with characteristically little heat left behind in the substrate. In this regard, reference is sometimes made to the length scale over which heat may diffuse during the laser-pulse duration τ:

$$L_{th} = \sqrt{D\tau} \tag{1}$$

where L_{th} denotes the thermal scale length, and D represents the thermal diffusivity [4, 5, 22–24].

Together with this, in the case of linear absorption, the argument is made that energy from the laser is deposited as heat over another characteristic length scale, the optical absorption depth $L_{abs} = 1/\mu_a$, where μ_a is the linear absorption coefficient. If L_{abs} significantly exceeds L_{th}, then heat diffusion is relatively unimportant during laser irradiation, and the interaction is sometimes said to be 'thermally confined' [24].

Caveats remain, when using this relationship to identify the range of heat effects. For one, while the laser-deposited heat does not diffuse far during irradiation, the heat distribution will continue to relax following absorption. The characteristic length L_{th} is a self-similar scale length of diffusion, and, like the FWHM, it refers to a range established with reference to the peak of the distribution – it is the same whether the deposited heat is very slight or very great. Thus L_{th} should not be equated to a length over which heating has impact, in a material or in a biotissue. More precisely, what is physically more significant is the range over which the local specific heat or temperature at any time exceeds a material threshold – a latent heat of fusion, for instance. For biological processes, not only the instantaneous local temperature but also its whole time history is important, in context of the Arrhenius model [25].

A second caveat to make is that in non-scattering media the absorption length L_{abs} naturally is referred to the direction of laser propagation, whereas heat diffusion is not. For a focal spot smaller than L_{abs}, it should not be expected that thermal effects would be laterally confined to the zone irradiated.

Though the self-similar scale length L_{th} of heat diffusion is not a good metric for the range of thermal effects, it is critically important in a slightly different context: during the time of laser irradiation, heat diffuses into the medium by that scale length, and correctly gives an upper limit for the temperature gradient. Where the specific heat exceeds the heat of fusion, vaporization, or ionization, material may be removed, and the temperature gradient initially determines the pressure gradient that drives spallation or evaporative ablation.

In the case of sufficiently long laser pulses or cw irradiation, absorption and ablation may proceed together nearly in steady-state. For ultrafast laser pulses, the heated layer may be still very thin at the end of the irradiation, and hot, and the gradient in both temperature and pressure may be very large. This fundamentally alters the picture of how ablation and heating are connected, and is preserved in pulse-train burst mode of ultrafast irradiation.

In context of evaporative ablation of material, the average rate of material removal is limited by the average power of the laser. If a given fluence is delivered in pulses, the peak optical field strength increases as the pulse duration decreases, and non-linear optical ionization of the medium results. Beyond this point, linear absorption due to chromophores becomes irrelevant, and the generic characteristics of absorption in a plasma govern the interaction, i.e., ablation is plasma-mediated.

In the case of plasma-mediated ablation, the linear absorption depth found from $1/\mu_a$ is effectively replaced by the absorption length in a plasma. This depends importantly on the density characteristics of the plasma formed at the surface, which in turn depends sensitively on the laser pulse. For a pulse <1 ps duration, of reasonable intensity contrast, a good approximation is a dense plasma at the surface resembling a metallic mirror, albeit at an electron temperature for which $k_B T_e \sim 1$ eV. Absorption occurs over a skin depth of this plasma (typically ~5–10 nm), which depends on temperature, density, and laser wavelength. Given such a small optical absorption depth, the thickness of the heated layer may instead be determined by thermal diffusion during the laser pulse, characterized by L_{th}. For a 1 ps pulse and metal-like thermal diffusivity ($D \sim 7 \times 10^{-5}$ m^{2}s^{-1}), this is ~20 nm.

The speed of the rarefaction wave of ablation in the dense heated material is governed by the ion-acoustic speed, c_s, which increases with temperature:

$$c_S = \sqrt{\frac{\gamma_e k_B T_e + \gamma_i Z k_B T_i}{M}} \tag{2}$$

where γ_e and γ_i are the adiabatic indices for the electrons and ions, k_B is the Boltzmann constant, T_e and T_i are the electron and ion temperatures, and M the ion mass. For a $k_B T_e = 1$ eV plasma of $M \sim 20$ a.m.u., it has a value of a few thousand meters per second.
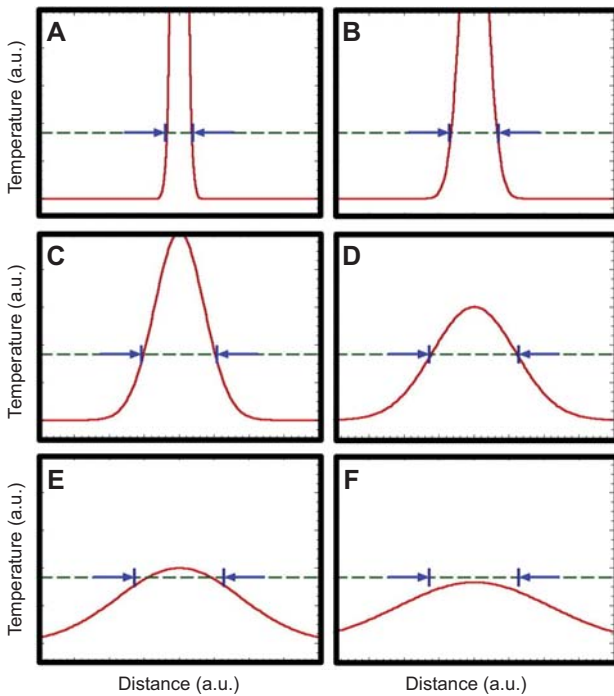
In effect, the heat source remains in contact with the substrate for about the time it takes for the rarefaction wave to erode the heated layer; this time can be very small, and the heat diffused into the substrate nearly negligible as a result. Instead of diffusing as heat into the substrate, the energy absorbed into the thin plasma layer is quickly converted to directed kinetic energy of expansion, and largely decouples from the substrate. Effectively, the heating of the substrate is minimized by an efficient ablative quenching. For the example above, the ablative quenching time is ~10 ps.

This picture carries over to pulse-train burst ultrafast ablation, with small modifications: the process of ionization may not need to begin again with each pulse, if there is persistence of even low density of plasma; and the gradient of the plasma density may be affected likewise by what tenuous plasma does persist on a nanosecond timescale between pulses. Characterization of this depends on further experiments.

4.3 Range of residual heat

As discussed above, the characteristic range over which a material or biotissue is affected is not found from the self-similar scale length of Eqn. (1) – as Figure 10 illustrates, despite the 1-ps timescale of irradiation.

Heuristically, consider Figure 16 depicting heat deposited initially in a Gaussian distribution in one dimension. It will diffuse as a Gaussian of increasing width and decreasing amplitude, keeping the area under the curve constant (assuming no energy loss). At any moment, a range of impact can be defined (arrows in Figure 16) as
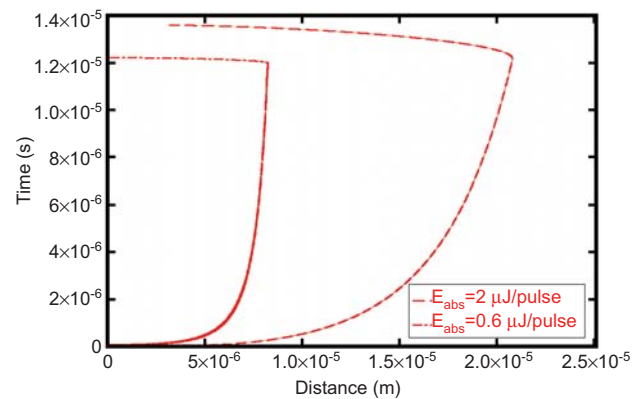
the extent over which the specific heat (or temperature profile) exceeds the threshold for a specific effect under consideration, such as melting. For a heated spot well exceeding this threshold, initially this radius increases, following the spreading temperature profile; later the decreasing amplitude begins to drop everywhere below threshold, and the limit point where the threshold condition is met shrinks. The range of the effect is then the largest range, in time, of all ranges for which the threshold is met.

The hole sizes produced in aluminum, in the series of Figure 10, can be matched by finding – over a family of equal-area Gaussians – the maximum radius for which the specific energy threshold is met, viz.:

$$r_{max} = \sqrt{\frac{E_0}{l Q_{sp} e}} \tag{3}$$

where E_0 is the net absorbed energy, l is the thickness over which the energy is absorbed (100 μm in Figure 10), Q_{sp} is the latent heat of vaporization (J cm^3) and e is Euler's number. This depends of course on the amount of heat left in the substrate after ablative quenching.

The overall picture is made more clear in Figure 17, a simulation of thermal diffusion in aluminum following irradiation by a 12-μs train of 1-ps pulses focussed to a 5-μm radius Gaussian spot; this simple illustrative model includes no hydrodynamics, and assumes constant absorption efficiency. Two different absorbed energies are compared, corresponding to different irradiation conditions, or to two absorption efficiencies. The trajectory of the simulation shows the radius at any time within which the temperature exceeds the melting point of aluminum. The two melt-diameters of Figure 17 are roughly

Figure 16 Schematic illustration of thermal diffusion of a Gaussian temperature distribution (heat vs. space) over time (from A to F): where a threshold effect (e.g., necrosis, specific heat of fusion), is the reference, the FWHM of a heat distribution is not relevant in characterizing range of impact. Rather, as a Gaussian relaxes in time a maximum width (arrows in A–F), measured at the threshold (dashed green line), is established, after which the distribution drops everywhere below significance.

Figure 17 Simulation of thermal diffusion in aluminum following irradiation by a 12-μs train of 1-ps pulses, and assuming two possible absorbed energies. In each, the trajectory follows in time the maximum radius at which the temperature exceeds the melting point of aluminum.

15 µm and 44 µm, to compare to the 30 µm hole-diameter in Figure 10.

5 Conclusions

Pulse-train burst treatment of materials or biotissues employs two characteristic timescales – pulse duration, and inter-pulse delay. Mixing the absorption and hydro-dynamic timescales associated with ultrafast laser pulses together with the thermal diffusion timescales of the nanosecond inter-pulse timing, makes for a new regime of interaction (Figure 18). The capacity follows, to control the accumulation of nearly negligible amounts of residual heat from ultrafast pulse to ultrafast pulse.

Because ultrafast-laser ablation is at intensities above the optical breakdown threshold, the details of linear absorption in a particular medium – metal, dielectric or tissue – are not immediately important. Except possibly in the initial optical breakdown, and generation of plasma, absorption by intrinsic chromophores is not significant. And for the question of 'thermal confinement', ultrafast-laser plasma-mediated absorption is also generic: for intense pulses of ~1 ps or less, plasma absorption and ablative quenching are nearly universal, and collateral heating is small because on a thermal-diffusion timescale, the absorbed energy largely is converted to kinetic energy of expansion of a thin layer from the surface, and thermally decouples from the substrate. Nonetheless, on a nanosecond timescale between pulses, and a microsecond timescale of the pulse-train burst,

small amounts of heat left in the specimen after each laser pulse can accumulate.

As a consequence, the pulse-train burst method can ablate at a per-pulse fluence which is below the nominal threshold for single-pulse ablation [12]. Thus, these sub-threshold pulses can collectively etch a material at rapid rates while at very gentle fluences. It appears likely that some number of sub-threshold pulses at the beginning of a pulse-train burst do not substantially ablate dentin, but instead contribute to preconditioning the material, perhaps slowly incubating a mediating plasma which persists from pulse to pulse, adding a new temporary linear absorption useful in etching a dielectric.

The mechanical, thermal, and thermodynamic, characteristics of a given substrate remain important of course. There are essential distinctions between processing metals and the treatment of teeth, though because glass and teeth are both dielectrics, there is a wealth of behavior in common between them. Studies in fused silica and ceramics are instructive for treatments of teeth; changes in structure are evident in the modified or recast material around an ablation feature, as seen in both cases by MRS.

For dentin, micro-Raman analysis revealed that the chemical composition of the flowed or recast dentin has changed significantly after laser irradiation. With longer pulse-train burst durations, organic components are effectively carbonized or evaporated, and dentin turns into an enamel-like material, glassy smooth in appearance and exhibiting the micro-Raman signature of enamel. If controlled suitably, perhaps this process may prove useful for sealing the treated area of dentin during laser drilling. The control of heat deposited, combined with the gentle
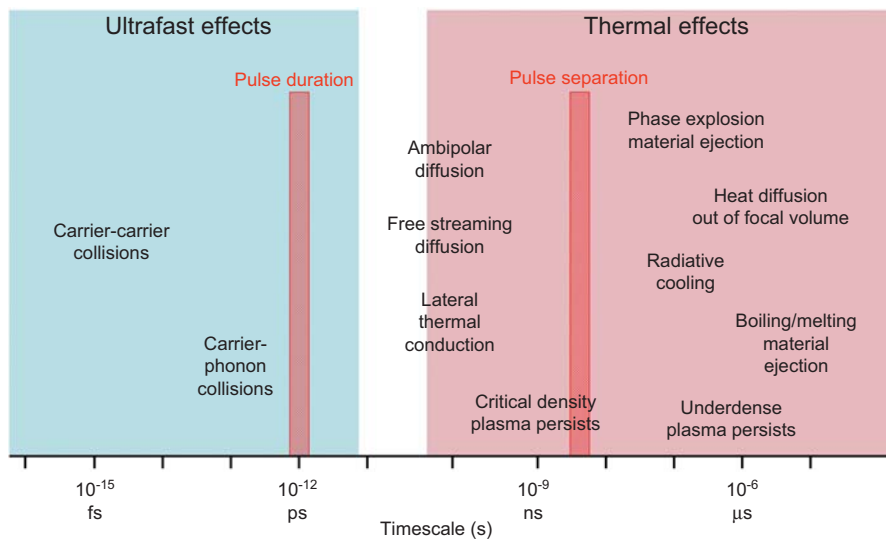
Figure 18 Schematic of pulse duration and inter-pulse separation of pulse-train bursts, in context of timescales for key physical processes affecting absorption and partitioning of energy in a solid.

ablation at rates comparable to mechanical tools, makes pulse-train burst machining a promising ancillary for dental surgery. Robust and compact laser systems currently under development are likely soon to provide 10–100 MHz pulse-train bursts at shot repetition rates >1 kHz or more. These will bring average etch rates to levels that are practical and attractive for clinical application.

In results on agar gels, serving as a proxy model for soft tissues, mechanical characteristics are a key in determining the impact of ultrafast burst-mode treatments. The short-lived plasma self-emission during laser irradiation makes clear that plasma-mediated ablation is very limited in hydrogel. Without a connective scaffold, the hydrogel lacks significant tensile strength, resulting in a cavitation void in the gel that forms and opens at the speed of a shockwave. Following the formation of this cavitation void, absorption into the plasma ceases, shutting down ablation. According to the timescale and lack of self-emission, it is much less plausible that material ejection and plasma-plume formation is what hinders absorption into the plasma.

Hydrogel ablation, therefore, reasonably reflects ablation in high-water-content soft tissue (e.g., renal tissue) that lacks a collagen matrix. Different results can be expected for connective tissues with a collagen matrix (as for differentiated organs) since the higher tensile strength will restrict cavitation, or cavitation will become anisotropic, and orientation of the laser axis to the collagen scaffold will become important. On high tensile material, such as dental hard tissue, it is observed that plasma self-emission lasts for the entire duration of the pulsetrain burst.

Significant questions remain about the ideal characteristics of an ultrafast-laser pulse-train burst for different interventions or therapies – the choice of inter-pulse spacing, the prospect of optimized intensity-envelopes tailored, say, for the ablation of teeth. These issues promise a higher degree of specific control of absorption, thermal diffusion, shockwave generation or secondary radiation, and answering them already shows the promise of clinical impact.

References

[1] Featherstone JD, Barrett-Vespone NA, Fried D, Kantorowitz Z, Seka W. CO_2 laser inhibitor of artificial caries-like lesion progression in dental enamel. J Dent Res 1998;77(6): 1397–403.

[2] Doukas AG, McAuliffe DJ, Flotte TJ. Biological effects of laser-induced shock waves: structural and functional cell damage in vitro. Ultrasound Med Biol 1993;19(2):137–46.

[3] Pronko PP, Dutta SK, Squier J, Rudd JV, Du D, Mourou G. Machining of sub-micron holes using a femtosecond laser at 800 nm. Opt Commun 1994;114(1–2):106–10.

[4] Neev J, Da Silva L, Feit M, Perry M, Rubenchik A, Stuart B. Ultrashort pulse lasers for hard tissue ablation. IEEE J Sel Top Quantum Electron 1996;2:790–800.

[5] Liu X, Du D, Mourou G. Laser ablation and micromachining with ultrashort laser pulses. IEEE J Quantum Electron 1997;33: 1706–16.

[6] Chichkov BN, Momma C, Nolte S, von Alvensleben F, Tünnermann A. Femtosecond, picosecond and nanosecond laser ablation of solids. Appl Phys A 1996;63:109–15.

[7] Rode AV, Gamaly EG, Luther-Davies B, Taylor BT, Graessel M, Dawes JM, Chan A, Lowe RM, Hannaford P. Precision ablation of dental enamel using a subpicosecond pulsed laser. Aust Dent J 2003;48(4):233–9.

[8] Niemz MH, Kasenbacher A, Strassl M, Bäcker A, Beyertt A, Nickel D, Giesen A. Tooth ablation using a CPA-free thin disk femtosecond laser aystem. Appl Phys B 2004;79(3): 269–71.

[9] Dela Rosa A, Sarma AV, Le CQ, Jones RS, Fried D. Peripheral thermal and mechanical damage to dentin with microsecond and sub-microsecond 9.6 μm, 2.79 μm, and 0.355 μm laser pulses. Lasers Surg Med 2004;35(3):214–28.

[10] Featherstone JDB, Fried D. Fundamental interactions of lasers with dental hard tissues. Med Laser Appl 2001;16(3): 181–94.

[11] Aminzadeh A, Shahabi S, Walsh LJ. Raman spectroscopic studies of CO_2 laser-irradiated human dental enamel. Spectrochim Acta A Mol Biomol Spectrosc 1999;55A(6): 1303–8.

[12] McKinney L, Frank F, Graper D, Dean J, Forrester P, Rioblanc M, Nantel M, Marjoribanks R. Mitigating intrinsic defects and laser damage using pulse-train burst (>100 MHz) ultrafast laser processing. Proc SPIE 2005;5970:59701L.

[13] Marjoribanks RS, Budnik FW, Zhao L, Kulcsár G, Stanier M, Mihaychuk J. High-contrast terawatt chirped-pulse-amplification laser that uses a 1-ps Nd: glass oscillator. Opt Lett 1993;18(5):361–3.

[14] MeX®, Alicona Imaging, Inc. <http://www.alicona.com/home/products/Mex/MeX_Brochure_07_08_Eng_small_res.pdf (Accessed June 11, 2012)>.

[15] Herman PR, Oettl A, Chen KP, Marjoribanks RS. Laser micromachining of transparent fused silica with 1-ps pulses and pulsetrains. Proc SPIE 1999;3616:148–55.

[16] Altshuler GB, Belikov AV, Sinelnik YA. A laser-abrasive method for the cutting of enamel and dentin. Lasers Surg Med 2001;28(5):435–44.

[17] Lenzner M, Rudolph W. Laser-induced optical breakdown in solids. In: Brabec T, editor. Strong field laser physics. New York: Springer; 2008, p. 243–60.

[18] Pérez-Gutiérrez FG, Camacho-López S, Aguilar G. Time-resolved study of the mechanical response of tissue phantoms to nanosecond laser pulses. J Biomed Opt 2011;16(11): 115001.

[19] Cherian AV, Rau KR. Pulsed-laser-induced damage in rat corneas: time-resolved imaging of physical effects and acute biological response. J Biomed Opt 2008;13(2):024009.

[20] Ali MF. Topical delivery and photodynamic evaluation of a multivesicular liposomal Rose Bengal. Lasers Med Sci 2011;26(2):267–75.

[21] Sramek C, Leung LS, Leng T, Brown J, Paulus YM, Schuele G, Palanker D. Improving the therapeutic window of retinal photocoagulation by spatial and temporal modulation of the laser beam. J Biomed Opt 2011;16(2):028004.

[22] Vogel A, Venugopalan V. Mechanisms of pulsed laser ablation of biological tissues. Chem Rev 2003;103(2):577–644.

[23] Vogel A, Noack J, Hüttmann G, Paltauf G. Mechanisms of femtosecond laser nanosurgery of biological cells and tissues. Appl. Phys B 2005;81:1015–47.

[24] Jacques SL. Role of tissue optics and pulse duration on tissue effects during high-power laser irradiation. Appl Opt 1993;32(13):2447–54.

[25] Thomsen S, Pearce JA. Thermal damage and rate processes in biologic tissues. In: Welch AJ, van Gemert MJC, editors. Optical-thermal response of laser-irradiated tissue. New York: Plenum Press; 1995, p. 487–550.